

1 **Technical note: Fu-Liou-Gu and Corti-Peter model performance evaluation for**
2 **radiative retrievals from cirrus clouds**

3

4 S. Lolli^{1,2}, J. R. Campbell³, J. Lewis¹, Y. Gu⁴, E. J. Welton⁵

5 ¹NASA GSFC-JCET, Code 612, 20771 Greenbelt, MD, USA

6 ² CNR-IMAA, Istituto di Metodologie per l'Analisi Ambientale, Potenza, Italy

7 ³ Naval Research Laboratory, Monterey, CA, USA

8 ⁴ UCLA, Los Angeles, CA, USA

9 ⁵ NASA GSFC, Code 612, 20771 Greenbelt, MD, USA

10 *Corresponding author: slolli@umbc.edu*

11 **Abstract**

12 We compare, for the first time, the performance of a simplified atmospheric
13 radiative transfer algorithm package, the Corti-Peter (CP) model, versus the more
14 complex Fu-Liou-Gu (FLG) model, for resolving top-of-the-atmosphere radiative
15 forcing characteristics from single layer cirrus clouds obtained from the NASA Micro
16 Pulse Lidar Network database in 2010 and 2011 at Singapore and in Greenbelt,
17 Maryland, USA in 2012. Specifically, CP simplifies calculation of both clear-sky
18 longwave and shortwave radiation through regression analysis applied to radiative
19 calculations, which contributes significantly to differences between the two. The
20 results of the intercomparison show that differences in annual net TOA cloud
21 radiative forcing can reach 65%. This is particularly true when land surface
22 temperatures are warmer than 288 K, where the CP regression analysis becomes
23 less accurate. CP proves useful for first-order estimates of TOA cirrus cloud forcing,

- 24 but may not be suitable for quantitative accuracy, including the absolute sign of
- 25 cirrus cloud daytime TOA forcing that can readily oscillate around zero globally.

26 **1. Introduction**

27 Cirrus clouds play a fundamental role in atmospheric radiation balance and their net
28 radiative effect remains unclear (IPCC 2013; Berry and Mace 2014; Campbell et al.
29 2016; Lolli et al. 2017). Feedbacks between cirrus dynamic, microphysical and
30 radiative processes are poorly understood, with ramifications across a host of
31 modeling interests and temporal/spatial scales (Liou 1985; Khvorostyanov and
32 Sassen 1998). Simply put, different models parameterize ice formation in varied, yet
33 relatively simplified, ways that impact how cirrus are resolved, and how their
34 macro/microphysical and radiative properties are coupled with other atmospheric
35 processes (e.g., Comstock et al. 2001; Immler et al. 2008). Consequently, models are
36 very sensitive to small changes in cirrus parameterization (Soden and Donner 1994;
37 Min et al. 2010; Dionisi et al., 2013).

38 Cirrus clouds are the only tropospheric cloud genus that either exerts a
39 positive or negative top-of-the-atmosphere (TOA) cloud radiative forcing effect
40 (CRE) during daytime. All other clouds exert a negative daytime TOA CRE. Cirrus
41 clouds exerting negative net TOA CRE cool the earth-atmosphere system and
42 surface below them. This occurs as the solar albedo term is greater than the
43 infrared absorption and re-emission term. Positive forcing occurs when the two are
44 reversed and infrared warming and re-emission exceed scattering back to space. In
45 contrast, all clouds cause a positive nighttime TOA value, with an infrared term
46 alone and no compensating solar albedo term. This dual property makes cirrus
47 distinct, and why it's crucial to understand how well radiative transfer models are
48 resolving their TOA CRE properties.

49 The burgeoning satellite and ground-based era of atmospheric monitoring
50 (Sassen and Campbell 2001; Campbell et al. 2002; Welton et al. 2002; Nazaryan, et
51 al. 2008; Sassen et al. 2008) has led to a wealth of new data for looking at global
52 cirrus cloud properties. In particular, TOA CRE, or at the surface (SFC), are evaluated
53 by means of radiative transfer modeling, designed with different degrees of
54 complexity. What is not yet known is how the relative simplicity of some models
55 translates to a relative retrieval uncertainty, given that the CRE effect of cirrus
56 clouds, at both the ground and TOA, are typically on the order of 1 W m^{-2} (e.g.,
57 Campbell et al. 2016; Lolli et al. 2017). Whereas some studies show the relative
58 uncertainty of such models as static percentages (Corti and Peter, 2009), the
59 absolute magnitude of uncertainty with respect to cirrus CRE is necessary to
60 understand whether or not they fit within acceptable tolerance thresholds sufficient
61 for quantitative use. Further, given the sensitivity in the sign of net annual cirrus
62 cloud daytime TOA CRE specifically (Campbell et al. 2016), it's plausible that some
63 simpler models are routinely aliasing positive versus negative TOA CRE.

64 Corti and Peter (2009; CP) describe a simplified radiative transfer model that
65 relies upon a constrained number of input parameters, including surface
66 temperature, cloud top temperature, surface albedo, layer cloud optical depth, and
67 the solar zenith angle. CP simplifies drastically the framework of the Fu-Liou-Gu
68 radiative transfer model (Fu and Liou 1992; Gu et al. 2003; Gu et al., 2011; FLG), for
69 instance, through a parameterization of the longwave and shortwave fluxes derived
70 from the FLG model calculations for realistic atmospheric conditions. Moreover, CP
71 does not directly consider gaseous absorption. The model has increasingly been

72 used to assess cirrus cloud radiative effects (Kothe et al. 2011; Kienast-Sjögren et al.
73 2016; Burgeois et al. 2016) from lidar measurements, owing to its relative simplicity
74 and lower computational burden compared with a model like FLG.

75 To date, CP model performance vs. FLG model has been evaluated for
76 sensitivities only to simulated synthetic clouds and never on real measurements,
77 especially those collected over long periods (Corti and Peter 2009). Such evaluation,
78 however, can readily be conducted using the unique NASA Micro Pulse Lidar
79 Network (MPLNET; Welton et al. 2002; Campbell et al. 2002; Lolli et al. 2013; Lolli
80 et al., 2014), established in 1999 to continuously monitor cloud and aerosol physical
81 properties (Wang et al., 2012, Pani et al., 2016).

82 The objective of this technical note is to then assess differences between CP
83 and FLG in terms of net annual daytime TOA CRE. CP and FLG model performance
84 are evaluated using MPLNET datasets collected from Singapore in 2010 and 2011, a
85 permanent tropical MPLNET observational site, and at Greenbelt, Maryland in 2012,
86 a midlatitude site. Our goal is to more appropriately characterize the sensitivities of
87 CP relative to what is generally considered a more complex, and presumably more
88 accurate, model, with the hopes of better understanding relative uncertainties, and
89 thus interpreting whether such uncertainties are appropriate for long-term global
90 cirrus cloud analysis.

91

92 **2. Method**

93 FLG is a combination of the delta four-stream approximation for solar flux
94 calculations (Liou et al. 1988) and a delta-two-four-stream approximation for IR

95 flux calculations (Fu et al. 1997), divided into 6 and 12 bands, respectively. It has
96 been extensively used to assess net cirrus cloud daytime radiative effects, most
97 recently for daytime TOA forcing characteristics within MPLNET datasets at both
98 Greenbelt, Maryland and Singapore, respectively (Campbell et al. 2016; Lolli et al.
99 2017). The results from these studies have led to the hypothesis of a meridional
100 gradient in cirrus cloud daytime TOA radiative forcing existing, with daytime cirrus
101 clouds producing a positive daytime TOA CRE at lower latitudes that reverses to a
102 net negative daytime TOA CRE approaching the non-snow and ice-covered polar
103 regions. They estimate absolute net cirrus daytime TOA forcing term between 0.03
104 and 0.27 $W m^{-2}$ over land at the mid-latitude site, which ranges annually between
105 2.20 - 2.59 $W m^{-2}$ at Singapore. The key here to this phenomenon is the possible
106 oscillation of the net daytime TOA CRE term about zero, which is believed to vary by
107 a maximum +/- 2 $W m^{-2}$ in absolute terms (i.e. normalized for relative cirrus cloud
108 occurrence rate and total daytime percentage locally), after accounting for polar
109 clouds that should be net cooling elements and varying surface albedos over land
110 and water exclusively (i.e., not ice). Resolving such processes thus requires
111 relatively high accuracy in radiative transfer simulations.

112 To calculate daytime cirrus cloud radiative effects from MPLNET datasets,
113 the lidar-retrieved single layer cirrus cloud extinction profile (Campbell et al. 2016;
114 Lewis et al., 2016, Lolli et al., 2016, Lolli et al., 2017) is transformed into crystal size
115 diameter (using the atmospheric temperature profile) and ice water content (*IWC*)
116 profiles using the parameterization proposed by Heymsfield et al. (2014). Those
117 parameters, at each range bin, are input into FLG. The thermodynamic atmospheric

118 profiles, together with ozone concentrations are obtained with a temporal
119 resolution of +/- 3 hr, from a meteorological reanalysis of the NASA Goddard Earth
120 Observing System Model Version 5.9.12 (GEOS-5). In contrast, for a given cloud case,
121 the corresponding cloud and atmospheric CP input parameters are explicitly the
122 land/ocean surface temperature, the cloud top temperature, the surface albedo, the
123 cloud optical depth for the specific layer and the solar zenith angle.

124 Calculations here are performed for the same MPLNET observational sites,
125 Singapore and Greenbelt, Maryland (i.e., NASA Goddard Space Flight Center; GSFC).
126 For the former site, two different values of the surface albedo, which is a common
127 input parameter in both models, are fixed at 0.12 and 0.05, respectively, as
128 Singapore is a metropolitan area completely surrounded by sea. This allows us to
129 more reasonably characterize forcing over the broader archipelago of Southeast
130 Asia, and follows the experiments described by Lolli et al. (2017). . At NASA GSFC,
131 only a single over-land albedo is used, though one that varies monthly between
132 0.12-0.15 based on climatology.

133 Here, we reconsider these results by first intercomparing those solved with
134 FLG and CP for net daytime TOA CRE over a practical range of cloud optical depth
135 (COD). As described in both Campbell et al. (2016) and Lolli et al. (2017), daytime is
136 specifically defined in these experiments as those hours where incoming net solar
137 energy exceeds that outgoing. Only under such circumstances can the net TOA CRE
138 term become negative. Otherwise, it is effectively nighttime, as the term is positive
139 and all clouds induce a warming TOA term. Those nighttime results presented
140 within the analysis below will instead be considered as context for understanding

141 net diurnally-averaged differences between the models specifically for the GSFC
142 dataset.

143

144 **3. Intercomparisons**

145 The daytime cirrus net TOA CRE, normalized by corresponding occurrence
146 frequency, in this case as a function of COD, was evaluated at Singapore (1.3 N, 103.8
147 E, 20 m above mean sea level) and GSFC (38.9 N, 76.8 W, 39 m above mean sea
148 level) for both FLG and CP. The method to estimate MPLNET cirrus cloud optical
149 properties is described in Lewis et al. (2015) and Campbell et al. (2016), for both 20
150 and 30 sr solutions from the unconstrained single-wavelength elastic lidar equation
151 at 532 nm (Campbell et al. 2016). The latter constraint provides “bookend”
152 estimates for TOA CRE designed to approximate system variance. For both models,
153 the daytime cirrus cloud net TOA CRE is calculated as the difference of two model
154 computations using different assumed states (cloudy sky minus cloud and aerosol
155 particulate-free conditions) to isolate the distinct cirrus cloud impact alone (in $W m^{-2}$).
156 2).

157 *3.1 Model sensitivities*

158 An initial sensitivity study was carried out to evaluate how the input
159 parameters, and eventually their uncertainties, influence the net TOA CRE
160 calculations. Results are summarized in Table 1. Model input parameter
161 sensitivities were investigated for surface albedo, COD, land/ocean surface
162 temperature and cloud top temperature. Table 1 shows how much net, SW and LW
163 fluxes change by varying each individual parameter alone. For instance, changing

164 the surface albedo from 0.12 to 0.14 and keeping the other three parameters fixed
165 produces similar changes in both models (26% for CP model and 25% for FLG
166 model). Changing COD from 1 to 1.1 produces a change of 16% for CP and 21% for
167 FLG. Changing surface temperature and cloud top temperature of 1K produces
168 respective changes of 10% and 7% for CP and 7% and 6% for FLG. Though subtle,
169 the models exhibit some differences in variance relative to the input parameters
170 required to initialize them.

171

172 *3.2 Singapore (2010-2011)*

173 FLG and CP were compared over a total of 33072 total daytime single layer
174 cirrus clouds at Singapore from 2010 to 2011. Figures 1, 2, 3 and 4 reflect
175 histograms of cirrus cloud relative frequency and net annual daytime TOA CRE
176 normalized by corresponding frequency, for both surface albedo values of 0.05 (Fig.
177 3 and 4; i.e., over sea) and 0.12 (Fig. 1 and 2; i.e. over land) at 0.03 COD resolution
178 from 0 to 3. This latter COD range was chosen to distinguish cirrus clouds in a
179 phenomenological manner consistent with Sassen and Cho (1992). Note, since a
180 common cloud sample is used, the 20 sr samples vary in COD between only 0 and
181 approximately 1 in contrast to the 30 sr sample topping out at 3. The observed
182 differences in net radiative effect can be ascribed to the different lidar ratio. Overall,
183 the results here complement the work of Berry and Mace (2014), who first
184 recognized the significance of optically-thin cirrus influencing the net normalized
185 term so significantly.

186 Intercomparison of net daytime TOA CRE vs. COD over the ocean at 30 sr, we
187 obtain -0.89 W m^{-2} from CP and -0.37 W m^{-2} for FLG. The overall CP net TOA CRE is
188 greater in absolute magnitude than FLG by a maximum difference of 58%. This
189 value is obtained by taking the ratio between yearly CRE from FLG over CP and then
190 the percentage difference. Over land (urban environment), CP net daytime TOA CRE
191 are higher than the FLG model by 25% (CP= 4.43 W m^{-2} and FLG= 3.35 W m^{-2}). The
192 COD value at which cirrus begin cooling the earth-atmosphere system, moving
193 toward higher COD, is systematically shifted towards higher values for CP with
194 respect to FLG.

195 To better understand the different outputs between the two models, a scatter
196 plot between from FLG barplot entries is shown in Figs. 2 and 4, and the
197 corresponding CP barplot values are plotted, over land and over ocean, in Figs. 5
198 and 6. The blue line represents the actual linear data regression, while the red line
199 represents an ideal case (i.e., slope=1, intercept=0). If the two radiative transfer
200 models show identical results regarding CRE, all the points should lie on the blue
201 line. The red line instead represents the actual regression line, or a relative measure
202 of how much the two models differ.

203 From Figs. 5 and 6, the FLG-derived net daytime CP TOA CRE values are
204 systematically greater in absolute value than the corresponding FLG values by 60%.
205 More in detail CP TOA CRE of 1 Wm^{-2} corresponds with FLG values ranging from
206 0.57 Wm^{-2} to 0.59 Wm^{-2} . On the contrary, the bias (or the intercept from the linear
207 regression) shows higher variability depending on the surface type underlying the
208 cirrus cloud (land versus ocean). This indicates that when a cirrus cloud shows a

209 neutral effect (0 Wm^{-2}) for CP model, FLG model solutions range from -0.05 (land)
210 to -1.1 Wm^{-2} (ocean). This implies that characterization of cirrus cloud warming or
211 cooling effects depend on the model.

212 For the sake of completeness, and to cover all the variability related to the
213 chosen LR, we performed the same analysis though excluding the 20 sr solution.
214 Over the ocean, we derive an overall forcing of 1.34 W m^{-2} for CP and 0.48 W m^{-2} for
215 FLG (41%). In Fig. 3 (blue arrow), a shift is clearly evident near 0.25 COD (0.6 for CP
216 and 0.35 for FLG) in CRE sign change (from positive to negative). Over land, we
217 estimated CP = 4.20 W m^{-2} and FLG = 2.98 W m^{-2} . (68%)

218

219 *3.4 Greenbelt, Maryland 2012*

220 To limit potential assessment ambiguity based on a single-site analysis, we
221 performed a second model comparison using the 2012 NASA GSFC dataset. A
222 summary of this dataset and net daytime TOA CRE results can be found in Campbell
223 et al. (2016). As this site is land-locked, only the single albedo was, again, used,
224 though varied monthly based on climatological passive satellite estimates. 21107
225 daytime cirrus cloud profiles were considered. Shown in Figure 6 (upper panel) are
226 the total net TOA CRE vs. COD at 30 sr, for CP (-2.59 Wm^{-2}) against FLG (0.05 Wm^{-2}).
227 A relative differencing here is impractical. Suffice however, this is a significant
228 difference, and the sign of the net daytime forcing term is uncertain when
229 comparing the two.

230 With this NASA GSFC dataset, we further consider an additional 32185
231 nighttime cirrus cloud cases within the analysis (Fig. 6, lower panel). Relative to

232 prior estimates of CP uncertainty compared with more complex models, a diurnal
233 average would be likely to produce a different, and plausibly closer, relative
234 agreement consistent with prior studies. That is, since during for most of the period
235 we define here as night there is no solar input, a simplification of the infrared
236 forcing terms and parameterizations alone would potentially yield a closer
237 comparison between the two models. For the NASA GSFC dataset, we solved a
238 relative net nighttime TOA CRE of 29.1 Wm^{-2} with FLG compared with 21.0 Wm^{-2}
239 with CP, or a relative difference approaching 50%. Summarized in Table 2 are the
240 discrepancies in terms of CRE at both observational sites.

241 It is useful at this point to discuss some of the potential elements driving
242 these differences. The larger discrepancies between the two models are likeliest
243 ascribed to the parameterization of three specific parameters in the CP model: the
244 first two, σ^* and k^* (Eq. 2 of Corti and Peter, 2009) are two approximated
245 parameters for the Stefan-Boltzmann constant and the surface temperature
246 exponent estimated from radiative calculations and used to calculate the outgoing
247 longwave earth radiation. The last parameter, γ^* (again obtained from a regression
248 analysis), is related to the asymmetry factor of cloud droplets and used to calculate
249 the cloud reflectance of shortwave radiation (Eq. 11 in Corti and Peter; 2009). We
250 speculate that, though the analysis is left to a future study on broader uncertainties
251 in modeling ice radiative properties inherently with any model, these parameters
252 are not the constants ascribed by CP, but that their values instead change with
253 respect to season and latitude.

254 The 20% relative model accuracy claimed in Corti and Peter (2009) may be
255 verified for special conditions in tropical latitudes, where the three parameters
256 discussed above are well optimized. But, that is clearly not found from our study.
257 Corti and Peters (2009) expressly stated that they used fixed values for those three
258 parameters (i.e., σ^* and k^* in Eq. 2 and γ^* in Eq. 11 in Corti e Peter, 2009) again
259 using regression analysis, but this shouldn't be the case, as net TOA CRF is very
260 sensitive to those parameters. For example, varying water vapor concentrations in
261 the atmosphere can be the responsible of a difference up to 25 Wm^{-2} (for
262 temperatures at the surface higher than 288K) in clear-sky earth longwave radiation
263 at Singapore, as stated in Corti and Peter (2009; Fig. 1). In our analysis we verified
264 that, over one year, the land surface temperature is higher than 288K 66% of the
265 time. For this reason, to assess if land surface temperature is responsible for these
266 larger discrepancies, we reproduced Fig. 6 (upper panel) masking out all cases
267 corresponding with land surface temperatures higher than 288 K at Greenbelt (in
268 Singapore those temperatures are mostly during nighttime). Shown in Figure 7 are
269 the results of the analysis. CP and FLG radiative transfer models in this range of
270 temperature are in much better agreement (NET CP = -8.06 Wm^{-2} ; NET FLG -8.65
271 Wm^{-2}), within 6%. Choosing surface temperatures lower than 288 K is reducing the
272 temperature gradient between the surface and cloud top, limiting the cloud thermal
273 warming effect (see Eq. 6 of Corti and Peter, 2009). Moreover, lower temperatures
274 are usually associated with higher solar zenith angle that implies stronger albedo
275 effects. For this reason, in Fig. 7 the albedo effect is outweighing the capacity of
276 cirrus cloud in trapping longwave radiation, with a net cooling effect estimated.

277 We advise that those looking to apply CP to long-term climate/cirrus cloud
278 study should carefully analyze the relevance of these settings to their given
279 experiment before directly applying the model, especially when land surface
280 temperatures are warmer than 288K.

281 **4. Conclusions**

282 Annual single-layer cirrus cloud top-of-the-atmosphere (TOA) radiative
283 effects (CRE) calculated from the Corti and Peter (2009) radiative transfer model
284 (CP) are compared with similar results from the more complex, and presumably
285 more accurate, Fu-Liou-Gu (FLG) radiative transfer model. The CP model calculates
286 CRE using a parameterization of longwave and shortwave fluxes that are derived
287 from real measurements optimized for a tropical environment through a regression
288 analysis to simplify the radiative calculations. Values for these parameterizations,
289 as suggested in Corti and Peter (2009), lead to relative differences in TOA CRE that
290 far exceed the stated 20% in the original manuscript. This includes parsing results
291 out for daytime, nighttime or diurnal averages. It is believed that specific
292 parameterizations with the simplified model cannot be considered global constants,
293 as originally defined for CP, but that they should be carefully evaluated on single
294 case basis for each experiment. Moreover we find that the land surface temperature
295 is responsible for significant discrepancies when larger than 288K, because the
296 original CP regression analysis is less accurate for larger temperatures. However, CP
297 uses less input parameters compared with FLG, making it practically and
298 computationally more efficient, particularly for large climate datasets. This is the
299 first time, however, that the two models are compared using long-term cirrus clouds

300 datasets, as opposed to synthetic datasets, with experiments conducted using NASA
301 Micro Pulse Lidar datasets collected at Singapore in 2010 and 2011 (Lolli et al.
302 2017) and Greenbelt, Maryland in 2012.

303 Net daytime TOA CRE was evaluated versus cloud optical depth (COD) for
304 steps of 0.03 (COD range: 0-1) at 20 sr and for steps of 0.1 at 30 sr (COD range: 0-3)
305 for Singapore datasets, while at 30 sr for Greenbelt, Maryland. Our findings suggest
306 that the difference in annual net TOA CRE between the two models approaches 65%
307 in one experiment at Singapore. At Greenbelt, Maryland, the sign of the net annual
308 daytime TOA CRE term differs, and the absolute difference varies between by nearly
309 2.5 Wm^{-2} . Differences in the sign of the net TOA forcing term, however, are most
310 worrying. Since cirrus clouds are the only cloud that can exhibit daytime positive or
311 negative net TOA CRE, subtle differences in absolute magnitude are less important
312 than whether or not the clouds are inducing a cooling or forcing term in the TOA
313 radiation budget.

314 In spite of this comparison, even if we reasonably speculate that FLG is the
315 more accurate model overall, because of its relative complexity compared with CP,
316 we are still missing regular comparisons of FLG with real observational data. Thus,
317 the practical gains to long-term application of a simplified model like CP cannot be
318 overstated, given lower computational demands. However, we believe that the
319 results from this study are noteworthy because they show that the differences
320 between the two models are significant. With respect to cirrus annual net daytime
321 TOA CRE, and given the perspective on their global distribution described by
322 Campbell et al. (2016) and Lolli et al. (2017), these sensitivities can lead to

323 completely different conclusions about global cirrus TOA forcing effects. Therefore,
324 in future work, it is imperative on the community to continue understanding and
325 refining the global parameterizations used in all radiative transfer models regarding
326 cirrus. Continued intercomparisons between models with real observation both at
327 ground (using flux measurements), in situ (aircraft measurements) and at TOA
328 (using satellite-based measurements,) remain critical interests.

329

330 **Acknowledgements**

331 This study and the NASA Micro Pulse Lidar Network (MPLNET) are supported by
332 the NASA Radiation Sciences Program (H. Maring). Author JRC acknowledges the
333 Naval Research Laboratory Base Program (BE033-03-45-T008-17) and support of
334 NASA Interagency Agreement NNG15JA17P on behalf of MPLNET.

335

336

337 **References**

- 338 Berry, E., and G. G. Mace, 2014: Cloud properties and radiative effects of the Asian
339 summer monsoon derived from A-Train data. *J. Geophys. Res. Atmos.*, 119,
340 doi:10.1002/2014JD021458.
- 341 Bourgeois, Q. *et al.* 2016: Ubiquity and impact of thin mid-level clouds in the tropics.
342 *Nat. Commun.* 7:12432 doi: 10.1038/ncomms12432
- 343 Campbell, S. Lolli J. Lewis, Y. Gu, E. Welton, 2016 “Daytime Cirrus Cloud Top-of-
344 Atmosphere Radiative Forcing Properties at a Midlatitude Site and their
345 Global Consequence” *J. Applied Meteor. Climat.*,
346 <http://dx.doi.org/10.1175/JAMC-D-15-0217.1>
- 347 Campbell, et al., 2002,” “Aerosol Lidar Observation at Atmospheric Radiation
348 Measurement Program Sites: Instrument and Data Processing”, *J. Atmos.*
349 *Oceanic Technol.*, 19, 431-442
- 350 Comstock, J.M., T.P. Ackerson (2001), G. G. Mace;,”Cirrus radiative properties in the
351 tropical western pacific. *Eleventh ARM Science Team Meeting Proceedings*,
352 Atlanta, Georgia, March 19-23.
- 353 Corti, T. and Peter, T., 2009: “A simple model for cloud radiative forcing”, *Atmos.*
354 *Chem. Phys.*, 9, 5751-5758, doi:10.5194/acp-9-5751-2009
- 355 Dionisi, D., Keckhut, P., Liberti, G. L., Cardillo, F., and Congeduti, F., 2013: Midlatitude
356 cirrus classification at Rome Tor Vergata through a multichannel Raman-
357 Mie-Rayleigh lidar, *Atmos. Chem. Phys.*, 13, 11853-11868, doi:10.5194/acp-
358 13-11853-2013.

359 Fu, Q., K. N. Liou, 1992, "On the correlated k -distribution method for radiative
360 transfer in nonhomogeneous atmospheres", *J. Atmos. Sci.*, 49, 2139–2156,
361 1992.

362 Gu, Y., J. Farrara, K. N. Liou, and C. R. Mechoso, 2003: Parameterization of cloud-
363 radiation processes in the UCLA general circulation model. *J. Climate*, 16,
364 3357-3370.

365 Gu, Y., K. N. Liou, S. C. Ou, and R. Fovell, 2011: Cirrus cloud simulations using WRF
366 with improved radiation parameterization and increased vertical resolution.
367 *J. Geophys. Res.* 116, D06119, doi:10.1029/2010JD014574

368 Heymsfield, A., D. Winker, M. Avery, M. Vaughan, G. Diskin, M. Deng, V. Mitev, and R.
369 Matthey, 2014: Relationships between ice water content and volume
370 extinction coefficient from in situ observations for temperatures from 0° to
371 –86°C: Implications for spaceborne lidar retrievals. *J. Appl. Meteor. Climatol.*,
372 53, 479–505

373 Immler, F., Treffeisen, R., Engelbart, D., Krüger, K., and Schrems, O. 2008: "Cirrus,
374 contrails, and ice supersaturated regions in high pressure systems at
375 northern mid latitudes", *Atmos. Chem. Phys.*, 8, 1689-1699, doi:10.5194/acp-
376 8-1689-2008.

377 IPCC: Climate Change 2013 – The Physical Science Basis, Working Group I
378 Contribution to the Fifth Assessment Report of the Intergovernmental Panel
379 on Climate Change, edited by: Inter- governmental Panel on Climate Change,
380 Cambridge University Press, Cambridge, UK and New York, NY, USA, 2014.

381 Khvorostyanov V. I. and K. Sassen, 1998: Cirrus Cloud Simulation Using Explicit
382 Microphysics and Radiation. Part I: Model Description. J. Atmos. Sci., 55,
383 1808–1821

384 Kienast-Sjögren, E., Rolf, C., Seifert, P., Krieger, U. K., Luo, B. P., Krämer, M., and Peter,
385 T.: Climatological and radiative properties of midlatitude cirrus clouds
386 derived by automatic evaluation of lidar measurements, Atmos. Chem. Phys.,
387 16, 7605-7621, doi:10.5194/acp-16-7605-2016, 2016.

388 Kothe, S., Dobler, A., Beck, A. and Ahrens, B., 2011. The radiation budget in a regional
389 climate model. *Climate dynamics*, 36(5-6), pp.1023-1036.

390 Kuo-Nan Liou, 1986: Influence of Cirrus Clouds on Weather and Climate Processes:
391 A Global Perspective. Mon. Wea. Rev., 114, 1167–1199.

392 Lolli, S., Campbell, J. R., Lewis, J. R., Gu, Y., Marquis, J. W., Chew, B. N., ... & Welton, E. J.
393 2017. Daytime Top-of-the-Atmosphere Cirrus Cloud Radiative Forcing
394 Properties at Singapore. *J. of App. Met. and Clim.*56(5), 1249-1257.

395 Lolli S., J. Lewis, R. Campbell, Y. Gu, E. Welton, 2016, “Cirrus Cloud Radiative
396 Characteristics from Continuous MPLNET Profiling at GSFC in 2012”, *Óptica*
397 *pura y aplicada*, Vol. 49 (1), 1-6,doi:10.7149/OPA.49.1.1.

398 Lolli S. et al, 2013a, “Evaluating light rain drop size estimates from multiwavelength
399 micropulse lidar network profiling,”*J. Atmos. Oceanic Technol.*, **30**, 2798–
400 2807.

401 Lolli S. et al. 2014. “High Spectral Resolution Lidar and MPLNET Micro Pulse Lidar
402 aerosol optical property retrieval intercomparison during the 2012 7-SEAS
403 field campaign at Singapore.” *Proc. SPIE 9246, Lidar Technologies*,

404 *Techniques, and Measurements for Atmospheric Remote Sensing X*, 92460C
405 (October 20, 2014); doi:10.1117/12.2067812.

406 Lewis, J. R., J. R. Campbell, P. C. Haftings and E. J. Welton, 2015: Overview and
407 analysis of the MPLNET Version 3 cloud detection algorithm. *J. Atmos.*
408 *Oceanic Technol.*, submitted

409 Min, M., P. Wang, J. R. Campbell, X. Zong, and Y. Li, 2010, “Midlatitude cirrus cloud
410 radiative forcing over China”, *J. Geophys. Res.*, 115, D20210,
411 doi:[10.1029/2010JD014161](https://doi.org/10.1029/2010JD014161).

412 Nazaryan, H., M. P. McCormick, and W. P. Menzel, 2008, “Global characterization of
413 cirrus clouds using CALIPSO data”, *J. Geophys. Res.*, 113, D16211,
414 doi:[10.1029/2007JD009481](https://doi.org/10.1029/2007JD009481).

415 Pani, S. K., S.-H. Wang, N.-H. Lin, S.-C. Tsay, S. Lolli, M.-T. Chuang, C.-T. Lee, S.
416 Chantara, and J.-Y. Yu, 2016” Assessment of aerosol optical property and
417 radiative effect for the layer decoupling cases over the northern South China
418 Sea during the 7-SEAS/Dongsha Experiment” *J. Geophys. Res. Atmos.*, 120,
419 doi: [10.1002/2015JD024601](https://doi.org/10.1002/2015JD024601)

420 Sassen, K. and J. R. Campbell, 2001: A Midlatitude Cirrus Cloud Climatology from the
421 Facility for Atmospheric Remote Sensing. Part I: Macrophysical and Synoptic
422 Properties. *J. Atmos. Sci.*, 58, 481–496,

423 Sassen, K., Z. Wang, and D. Liu, 2008, “Global distribution of cirrus clouds from
424 CloudSat/Cloud-Aerosol Lidar and Infrared Pathfinder Satellite
425 Observations (CALIPSO) measurements”, *J. Geophys. Res.*, 113, D00A12,
426 doi:[10.1029/2008JD009972](https://doi.org/10.1029/2008JD009972).

427 Soden, B. J., and L. J. Donner (1994), Evaluation of a GCM cirrus parameterization
428 using satellite observations, *J. Geophys. Res.*, 99(D7), 14401–14413,
429 doi:[10.1029/94JD00963](https://doi.org/10.1029/94JD00963).

430 Wang, S. H., S. Tsay, N. Lin, S. Chang, C. LI, E. J. Welton, B. N. Holben N. C. Hsu, W. K.
431 Lau, S. Lolli C. Kuo, H. Chia, C. Chiu, C. Lin, S. W. Bell, Q. Ji, R. A. Hansell, G.
432 Sheu, K. Chi, and C. Peng. 2012. "Origin, transport, and vertical distribution
433 of atmospheric pollutants over the northern South China Sea during the
434 7SEAS/Dongsha experiment." *Atmos. Environment*, Vol. 78, 124-133

435 Welton, E. J., et al., 2002: Measurements of aerosol vertical profiles and optical
436 properties during INDOEX 1999 using micropulse lidars. *J. Geophys. Res.*,
437 107, 8019,
438

439 **FIGURES**

440

441 **FIGURE 1** Analysis over land (Albedo=0.12) for 20sr solution. CRE vs. COD is
442 weighted by occurrence frequency for Corti and Peter(red) and FLG
443 (blue) models over 2010-2011

444

445 **FIGURE 2** Analysis over land (Albedo=0.12) for 30sr solution. CRE vs. COD is
446 weighted by occurrence frequency for Corti and Peter(red) and FLG
447 (blue) models on 2010-2011.

448

449 **FIGURE 3** Same as Figure 1, but over the ocean (Albedo=0.05). The arrow shows the
450 shift in COD for CRE sign change between the two models

451

452 **FIGURE 4** Same as Figure 2, but over the ocean (Albedo=0.05)

453

454 **FIGURE 5** Scatter plot and linear regression for 30sr solution for FLG and CP CRE in
455 2010-2011 over land (upper panel) and ocean (lower panel)

456

457 **FIGURE 6** Analysis on 2010 dataset from MPLNET GSFC observational site for 30sr
458 solution daytime (upper panel) and nighttime (lower panel).

459

460 **FIGURE 7** Same as Figure 6, taking out those measurements with a land surface
461 temperature $T_{\text{surf}} > 288\text{K}$

462

463

464

465

466 Tables

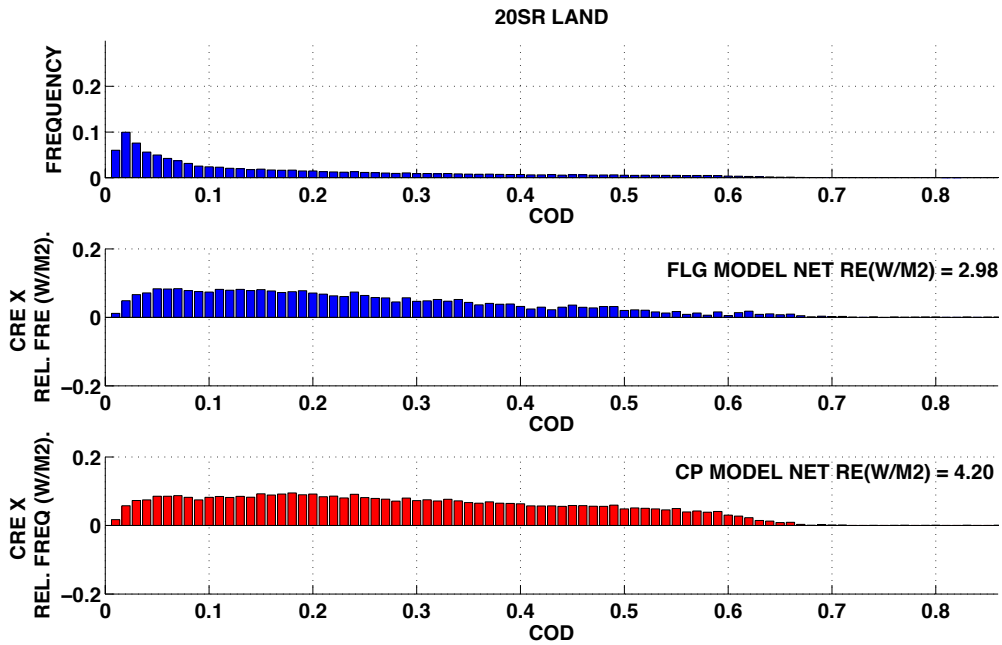
467

NET CP	NET FLG	LW TOA FLG	SW TOA FLG	LW TOA CP	SW TOA CP	
-12.6	-9.4	67.8	-77.2	69	-81.6	Ref
9.3 (26%)	-7 (25%)	67.8	-74.8	69	-78.3	Albedo
-14.7 (16%)	-11.4 (21%)	71.8	-83.2	73.5	-88.2	Cod
-11.3(10%)	-8.7(7%)	68.5	-77.2	70.3	-81.6	Surf Temp
-13.5(6%)	-10(5%)	67.2	-77.2	68.1	-81.6	Cl Top Temp

468 Table 1 Total NET, SW and LW fluxes (W/m^2) at TOA. Sensitivities of CP and FLG
 469 radiative transfer models with respect to the surface albedo, cloud optical depth
 470 Unperturbed parameters are COD=1, Surface albedo=0.12, $T_{surf}=294K$ Cloud top
 471 $T_{top}=229K$. The variation in net radiative forcing expressed in percentage for each
 472 parameter are calculated changing the surface albedo from 0.12 to 0.14, the COD
 473 from 1 to 1.1, and augmenting the temperatures of 1K.
 474

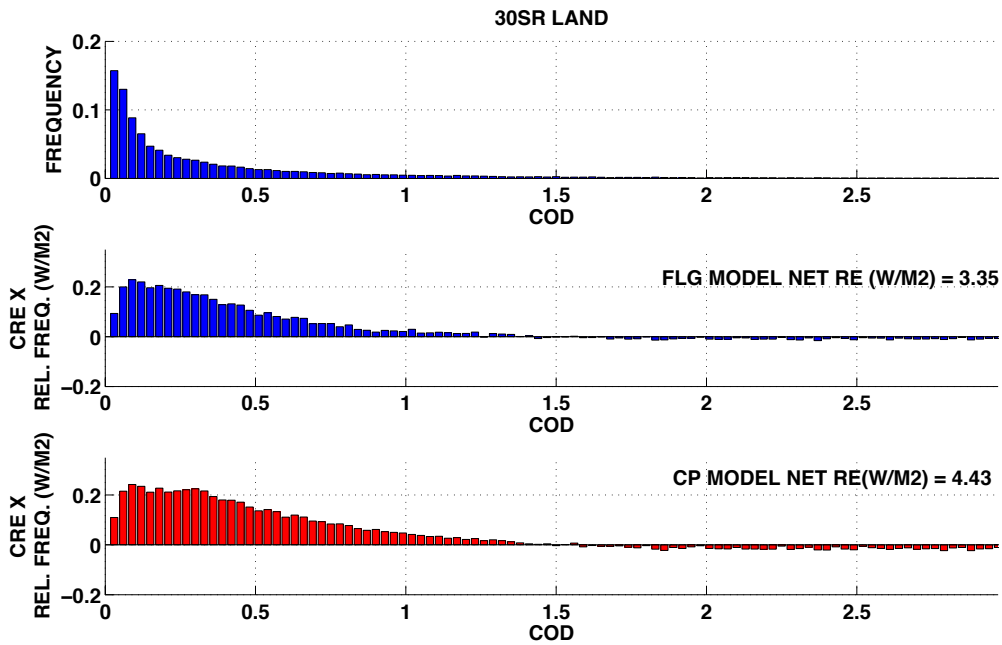
CRE vs. COD	Ocean	Land
SING 2010-2011	20sr CP=1.34 FLG=0.48(65%)	20sr CP=4.20 FLG=2.98 (30%)
	30sr CP=-0.89 FLG=-0.37 (58%)	30sr CP=4.43 FLG=3.35 (25%)
GSFC 2012		30sr CP=-2.59FLG=0.07

475 Table 2 Summary of principal CRE (Wm^{-2}) differences between FLG and CP radiative
 476 transfer model depending on year and on land/ocean.
 477



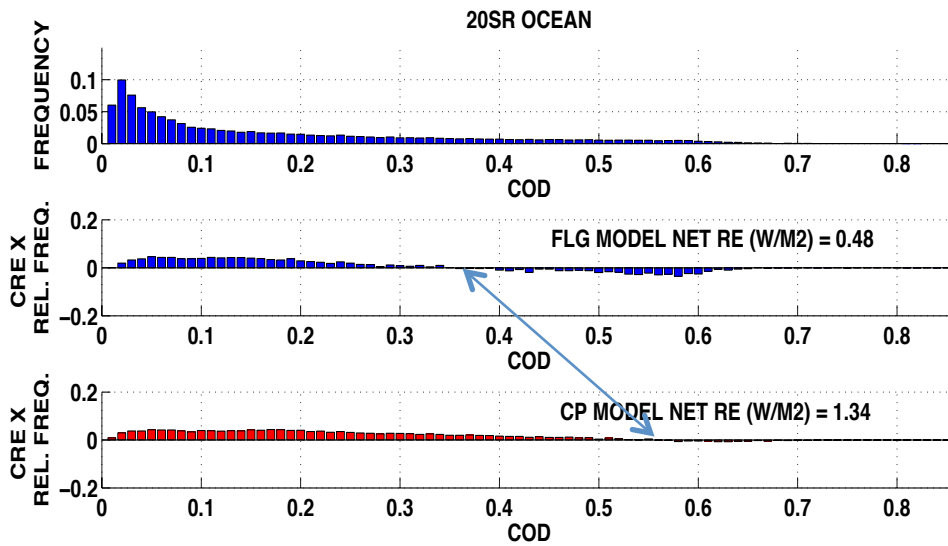
479

480 **Figure 1** Analysis over land (Albedo=0.12) for 20sr solution. CRE vs. COD is weighted by occurrence
 481 frequency for Corti and Peter(red) and FLG (blue) models over 2010-2011
 482

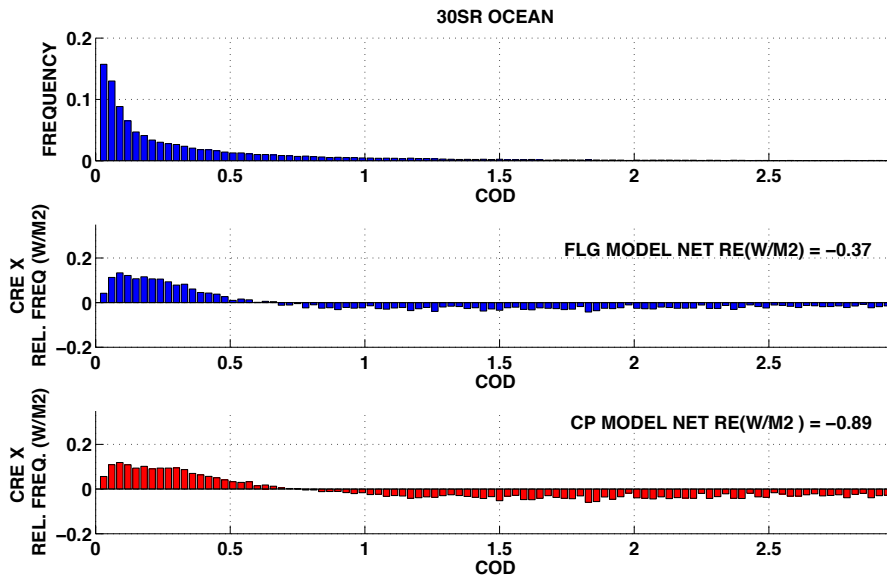


483

484 **Figure 2** Analysis over land (Albedo=0.12) for 30sr solution. CRE vs. COD is weighted by occurrence
 485 frequency for Corti and Peter(red) and FLG (blue) models on 2010-2011.
 486

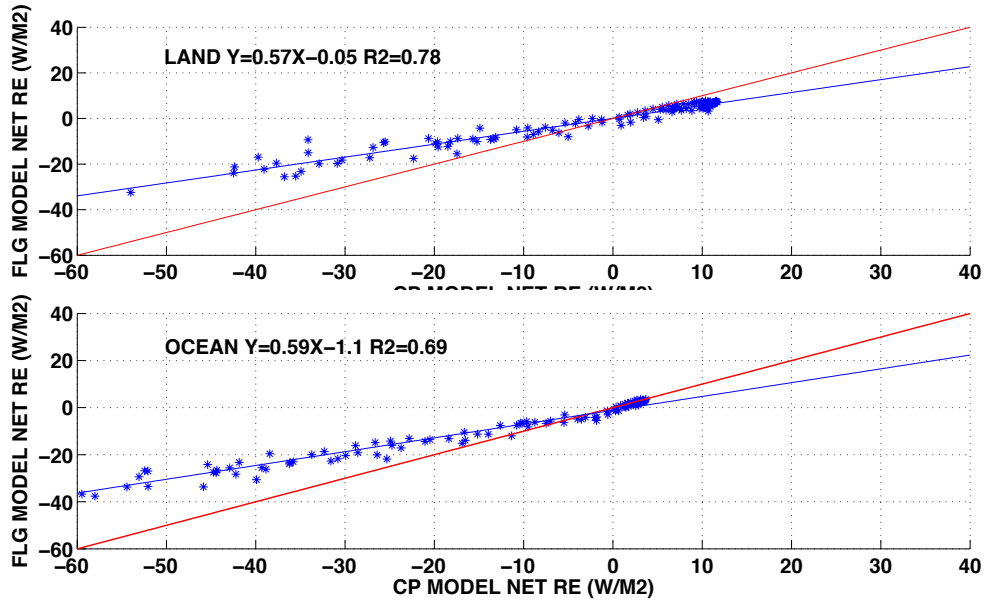


488 **Figure 3** Same as Figure 1, but over the ocean (Albedo=0.05) . The arrow shows the shift in COD for
 489 CRE sign change between the two models
 490



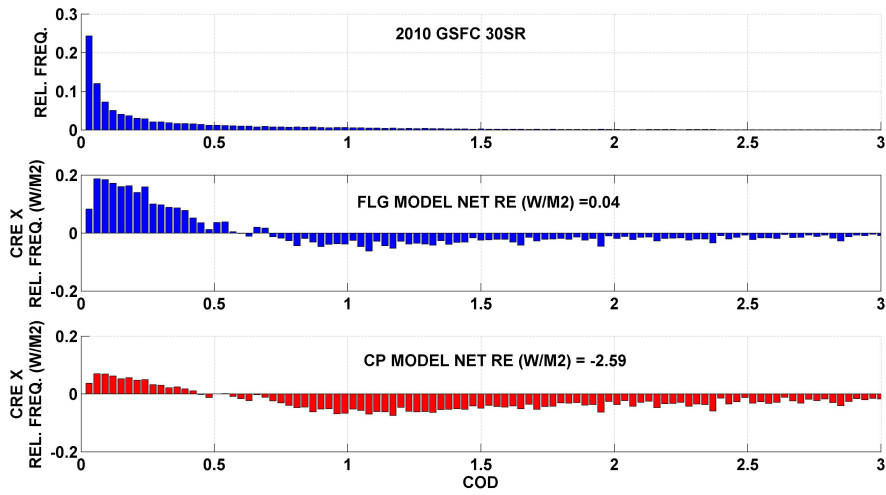
491
 492 **Figure 4** Same as Figure 2, but over the ocean (Albedo=0.05)
 493

494

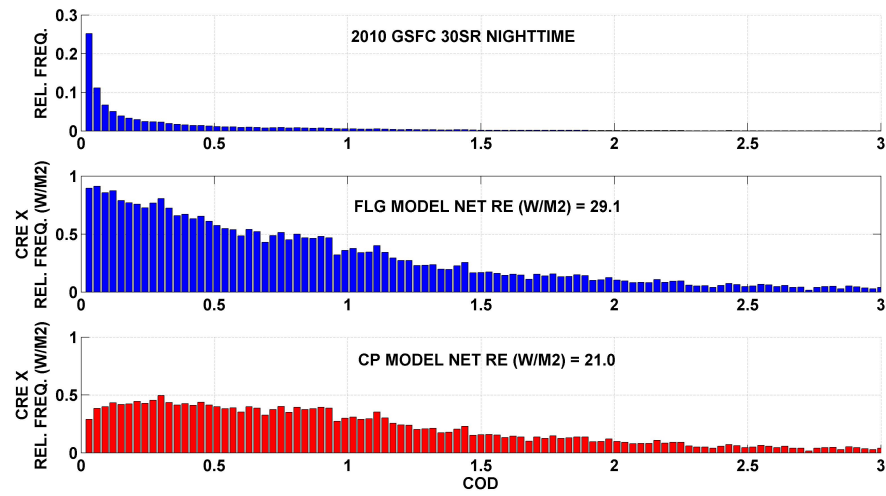


495
496
497
498
499
500

Figure 5 Scatter plot and linear regression for 30sr solution for FLG and CP CRE in 2010-2011 over land (upper panel) and ocean (lower panel)

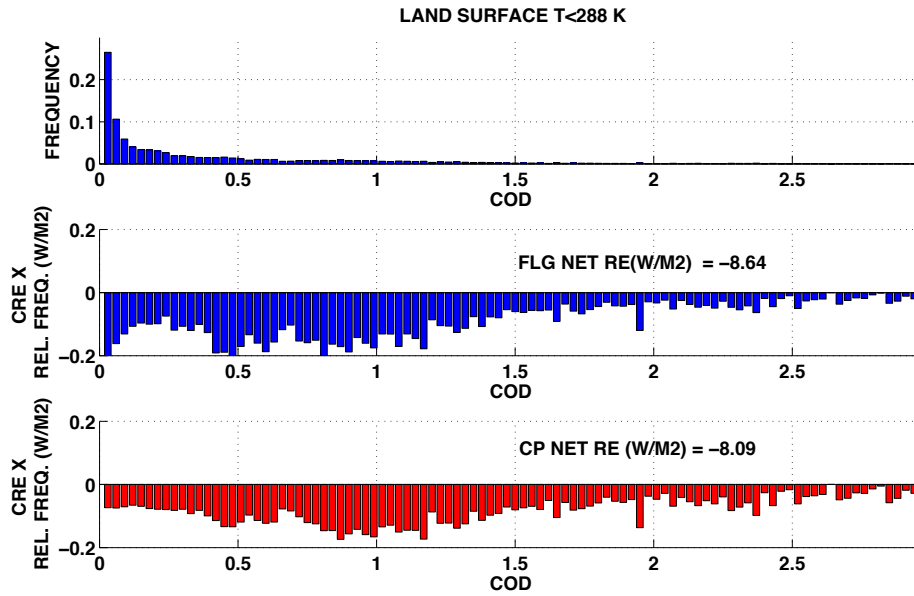


501



502
503
504
505
506

Figure 6 Analysis on 2010 dataset from MPLNET GSFC observational site for 30sr solution daytime (upper panel) and nighttime (lower panel).



507
 508
 509
 510

Figure 7 Same as Figure 6, taking out those measurements with a land surface temperature $T_{surf} > 288K$